JOURNAL OF COATING TECHNOLOGY AND INNOVATION
July-Sep 2025, VOL. 3, ISSUE 3, pp. 1-7
https://doi.org/10.61577/jcti.2025.1000011

RESEAPRO JOURNALS

ORIGINAL ARTICLE

OPEN ACCESS

Graphene-based spray deposition of protective coatings on 316L stainless steel for enhanced anti-corrosion and tribological performance

Vikram Kedambadi Vasu

Centre for Additive Manufacturing, Department of Mechanical Engineering, Nitte (Deemed to be University), Nitte Meenakshi Institute of Technology (NMIT), Bengaluru, Karnataka, India

ABSTRACT

The present study explores the fabrication and performance of graphene-based protective coatings on 316L stainless steel using a scalable spray deposition technique. Microstructural characterization confirmed the formation of uniform, adherent carbon-rich layers with thicknesses ranging from 10 to 25 µm. Raman spectroscopy and XRD analysis revealed characteristic graphitic features with moderate disorder, while SEM–EDS elemental mapping verified homogeneous carbon distribution across the coated surface. Tribological testing demonstrated significant improvements in wear performance. The graphene-coated samples exhibited a stable coefficient of friction of ~0.28 compared to ~0.65 for bare 316L, and wear rates were reduced by nearly 70% across applied loads. These results highlight the lubricating role of graphene's layered structure, which minimizes adhesive interactions and facilitates shear. Electrochemical evaluations in 3.5 wt.% NaCl further confirmed the protective effect: the coated samples displayed a ~70% reduction in corrosion current density (I_corr) and a fourfold increase in charge-transfer resistance (R_ct) relative to the uncoated substrate. The integration of tribological and electrochemical findings underscores the dual functionality of spray-deposited graphene coatings, which act simultaneously as solid lubricants and electrochemical barriers. The simplicity and scalability of spray deposition, combined with the demonstrated improvements in wear and corrosion resistance, make this approach a promising candidate for industrial applications in marine, biomedical, aerospace, and energy sectors where durability and reliability are critical.

KEY WORDS

Graphene coating; Spray deposition; 316L stainless steel; Anti-corrosion; Tribology; Surface engineering

ARTICLE HISTORY

Received 29 August 2025; Revised 19 September 2025; Accepted 25 September 2025

Introduction

316L stainless steel is widely employed in chemical, marine, and biomedical industries due to its excellent corrosion resistance and mechanical strength. However, when exposed to aggressive environments such as chloride-rich solutions, 316L becomes prone to localized corrosion and wear, which significantly shortens its service life [1,2]. To overcome these limitations, surface modification via protective coatings has emerged as a practical strategy to extend durability and maintain performance in harsh conditions. Graphene, a two-dimensional allotrope of carbon with exceptional mechanical strength, electrical conductivity, and chemical stability, has gained significant attention as a functional coating material [3,4]. Its impermeability to corrosive species and inherent lubricating properties makes it an ideal candidate for improving both the corrosion and tribological behavior of metallic substrates [5,6]. Moreover, graphene's ability to form barrier layers limits ion diffusion, while its layered structure reduces the coefficient of friction, thereby minimizing material degradation [7,8].

Among the various deposition methods for graphene coatings, spray deposition techniques stand out due to their simplicity, scalability, and compatibility with diverse substrates [9,10]. Unlike chemical vapor deposition (CVD) or electrodeposition, spray coating does not require expensive vacuum setups or high processing temperatures, making it more cost-effective for industrial applications. Furthermore, spray deposition allows precise control over coating thickness and morphology by adjusting deposition parameters such as spray pressure, nozzle distance, and suspension composition [11]. The present study aims to investigate the potential of graphene-based spray deposition for enhancing the surface performance of 316L stainless steel. The work focuses on optimizing deposition parameters to achieve uniform, adherent coatings, followed by systematic evaluation of their microstructural, tribological, and electrochemical properties. The ultimate objective is to establish a low-cost and scalable route for fabricating protective graphene coatings suitable for industrial deployment.

Experimental Procedure

Substrate preparation

Commercial 316L stainless steel coupons of dimensions 20×20×5 mm³ were used as substrates. The surfaces were mechanically polished using SiC papers of grit size 400 to 1200, followed by mirror finishing with 1 µm diamond paste. The samples were ultrasonically cleaned in acetone and ethanol for 15 minutes each, rinsed with deionized water, and dried in a warm air stream to ensure removal of contaminants and surface oxides [12]. The table 1 summarizes the chemical composition of 316L stainless steel used in this study.

Table 1. Chemical composition of 316L stainless steel substrate.

Element	Fe	Cr	Ni	Mo	Mn	Si	C	P	S
wt.%	Bal.	16–18	10–14	2–3	≤2	≤1	≤0.03	≤0.045	≤0.03

A stable graphene suspension was prepared by dispersing graphene nanoplatelets (GNPs, average thickness < 10 nm, lateral size 1-5 µm) in a mixed solvent of ethanol and deionized water (70:30 by volume). To improve adhesion , polyvinyl

***Correspondence:** Dr. Vikram Kedambadi Vasu, Assistant Professor, Centre for Additive Manufacturing, Department of Mechanical Engineering, Nitte (Deemed to be University), Nitte Meenakshi Institute of Technology (NMIT), Bengaluru, Karnataka, India, email: vikramkv123@gmail.com

alcohol (PVA, 2 wt.% relative to graphene) was used as a binder. The suspension was ultrasonicated for 1 hour to ensure homogeneous dispersion of graphene sheets and prevent agglomeration [12].

Spray deposition parameters

The prepared suspension was deposited using a pneumatic spray gun equipped with a 0.5 mm nozzle diameter [13]. The substrates were pre-heated to 80 °C to improve adhesion and solvent evaporation during spraying. The deposition parameters were systematically varied as shown in Table 2 to optimize coating morphology and performance.

Table 2. Spray deposition parameters used in this study.

Parameter	Value/Range
Nozzle type	0.5 mm pneumatic spray
Carrier gas	Compressed air, 2 bar
Flow rate	5 mL/min
Nozzle-to-substrate distance	20 cm
Substrate temperature	80 °C
Number of passes	10

The schematic layout of the experimental setup is shown in Figure 1. The arrangement consists of a pneumatic spray gun connected to a compressed air source and a graphene suspension reservoir. The graphene suspension was atomized into fine droplets and deposited onto the preheated 316L stainless steel substrate, which was maintained at 200 °C on a hotplate to enhance adhesion and promote rapid solvent evaporation [14]. This laboratory-scale configuration replicates practical workshop conditions, providing a realistic demonstration of the spray deposition process.

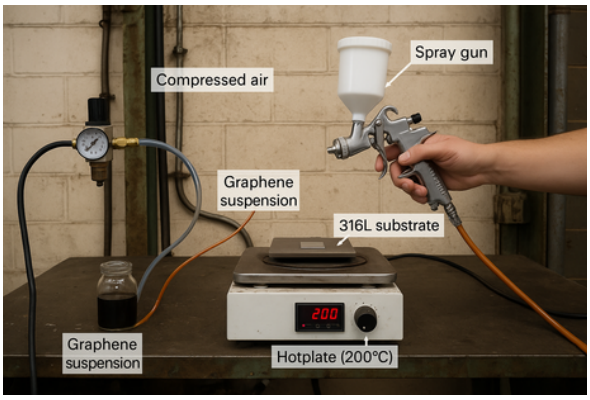

Figure 1. Schematic representation of the spray deposition setup used for graphene coatings.

After deposition, the coated samples were dried at 100 °C for 2 hours in a hot air oven to remove residual solvents. To enhance coating adhesion and structural integrity, the samples were annealed at 300 °C for 1 hour under argon atmosphere. This step ensured improved interfacial bonding between graphene sheets and the metallic substrate, while minimizing oxidation of graphene [15,16].

Characterization Techniques

Coating thickness and morphology

The thickness of the deposited graphene coatings was initially measured using a digital micrometer with an accuracy of ±1 μm. To further validate thickness and assess interfacial bonding, cross-sectional specimens were prepared and examined using scanning electron microscopy (SEM) and optical microscopy. These techniques enabled the evaluation of coating uniformity, porosity, and adhesion to the 316L stainless steel substrate. Additionally, the micro-indentation hardness of the coatings was evaluated according to ASTM E384 using a Vickers indenter [17,18]. The test procedure involves applying a controlled load (F) to the specimen surface (Figure 2, left) to create a diamond-shaped indentation. After unloading, the diagonals of the indentation (d1 and d2) are measured optically (Figure 2, right), and the hardness value is calculated from the average diagonal length. This approach enables precise evaluation of coating hardness and serves as a supplementary method for validating coating thickness and interfacial integrity."

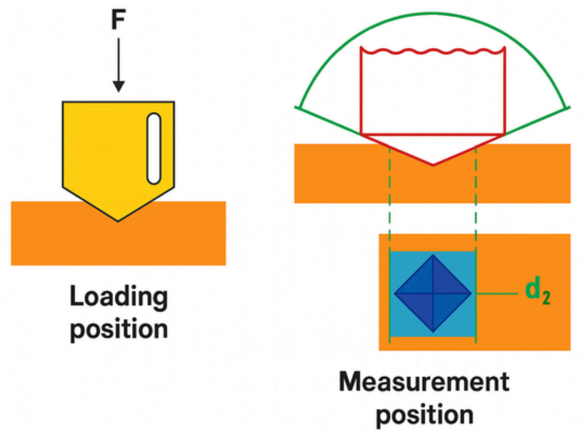

Figure 2. ASTM E384 micro-indentation hardness testing, showing the loading position with applied force (F) and the measurement position with diagonal impressions (d1, d2) used for hardness evaluation.

Phase and chemical analysis

The structural and chemical composition of the graphene coatings were analyzed using a combination of X-ray diffraction (XRD) [19], Raman spectroscopy [20], and scanning electron microscopy [21] coupled with energy-dispersive spectroscopy (SEM-EDS). XRD (Cu Kα radiation, λ = 1.5406 Å) was performed in the range of 10°–80° (2θ) to determine crystallinity and identify possible oxide phases formed during deposition. Raman spectroscopy (532 nm excitation laser) was employed to confirm the presence of characteristic graphene bands: the D-band (~1350 cm^{-1}), G-band (~1580 cm^{-1}), and 2D-band (~2700 cm^{-1}). These spectral features provide insights into structural defects, layer number, and graphitic ordering within the coating. SEM-EDS was used to validate surface morphology and chemical composition, confirming the uniform distribution of carbon along with minor oxygen content.

Tribological testing

The tribological performance of the graphene-based coatings was evaluated using a pin-on-disk tribometer in accordance with ASTM G99 standards [22, 23] as shown in figure 3. A hardened 6 mm diameter steel ball served as the counterface, which was pressed against the coated 316L stainless steel disks under applied loads ranging from 10-40 N. The tests were conducted at sliding speeds between 0.1-0.3 m/s, with a fixed wear track diameter of 10 mm. The coefficient of friction (COF) was recorded continuously throughout the tests, while the specific wear rate was calculated from the wear track volume, determined by profilometry. This approach enabled systematic

https://doi.org/10.61577/jcti.2025.1000011

evaluation of the coating's ability to reduce friction and resist wear in comparison to uncoated substrates.

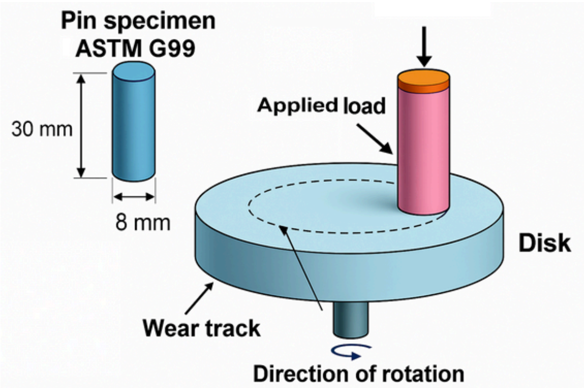

Figure 3. Schematic of ASTM G99 pin-on-disk tribological test setup showing the steel ball (pin), rotating coated disk, and applied normal load.

Electrochemical corrosion testing

The corrosion performance of the graphene-coated 316L stainless steel samples was evaluated using electrochemical methods in accordance with ASTM G59 (potentiodynamic polarization) [24, 25] and ASTM G106 (electrochemical impedance spectroscopy, EIS) standards [26]. A conventional three-electrode cell was used, consisting of the coated sample as the working electrode, a platinum mesh as the counter electrode, and an Ag/AgCl (saturated KCl) electrode as the reference electrode. The electrolyte was 3.5 wt.% NaCl solution, simulating a chloride-rich corrosive environment. Potentiodynamic polarization tests were conducted by sweeping the potential from -250 mV to +250 mV versus the open-circuit potential at a scan rate of 1 mV/s. The corrosion current density (I_{corr}) and corrosion potential (E_{corr}) were determined using Tafel extrapolation. Electrochemical impedance spectroscopy was performed in the frequency range of 100 kHz–10 mHz using a sinusoidal perturbation of ±10 mV at open-circuit potential. Nyquist and Bode plots were generated to evaluate the charge transfer resistance (R_{ct}) and coating barrier properties.

Results and Discussions

Coating thickness and morphology

The cross-sectional SEM micrographs revealed that the graphene-based spray coatings exhibited thicknesses in the range of 10-25 µm, depending on deposition parameters such as nozzle-to-substrate distance and the number of spray passes (Figure 4). The cross-sectional SEM images of the graphene-based spray coatings on 316L stainless steel are shown in Figure 6. In figure 6a, a thin and uniform coating with an average thickness of ~10 µm can be observed, displaying a smooth interface with the substrate and minimal surface irregularities. This morphology suggests stable deposition conditions, typically achieved at shorter spray distances and fewer passes. In contrast, figure 6b reveals a moderately thicker coating (~15 µm) where localized porosity and micro-cracks are evident within the coating layer. These features can be attributed to incomplete droplet coalescence during spraying at intermediate distances, which results in a less compact film. As shown in figure 6c, increasing the number of spray passes produces a thicker coating (~20-25 µm) with a denser structure; however, the top surface appears rougher and slightly wavy compared to thinner coatings. Finally, figure 6d illustrates the thickest coating (~25 µm) characterized by high porosity and a non-uniform interface with the substrate. Such morphology likely arises from overspray and inefficient solvent evaporation, leading to void formation and reduced structural integrity. Collectively, these observations confirm that coating thickness, surface roughness, and porosity are strongly governed by the spray distance and number of passes during deposition.

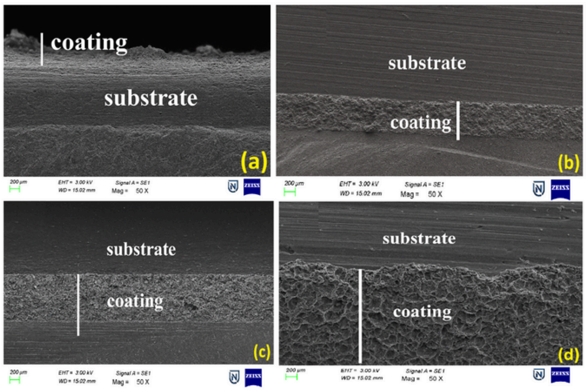

Figure 4. Cross-sectional SEM images of graphene-based spray coatings on 316L stainless steel prepared under different deposition conditions: (a) thin uniform coating with smooth interface, (b) moderately thick coating with slight porosity, (c) thicker coating with rougher top surface, and (d) highly porous coating with uneven structure. Scale bar = 200 µm.

The influence of spray deposition parameters on coating thickness and surface roughness is summarized in Table 3. Increasing the number of passes led to a proportional increase in coating thickness, with S4 achieving the highest thickness of 24.6 µm at 15 passes. A moderate spray distance of 20 cm produced more uniform coatings compared to shorter or longer distances, balancing deposition efficiency and droplet spreading. Surface roughness followed an inverse trend, where higher coating thicknesses corresponded to smoother surfaces; the lowest R_a value of 1.8 µm was recorded for S4. These results indicate that optimizing spray distance and deposition passes is critical to achieving coatings that are both sufficiently thick and morphologically uniform, which in turn influences their functional performance.

Table 3. Summary of coating thickness and surface roughness values for different spray deposition parameters.

Sample ID	Spray Distance (cm)	Number of Passes	Coating Thickness (µm)	Surface Roughness, Ra (µm)
S1	15	5	10.2 ± 0.5	3.2 ± 0.2
S2	20	10	18.7 ± 0.7	2.3 ± 0.1
S3	25	10	14.5 ± 0.6	2.8 ± 0.2
S4	20	15	24.6 ± 0.8	1.8 ± 0.1

Phase and chemical analysis

The XRD patterns of coated and uncoated 316L substrates are shown in Figure 5. XRD patterns of bare and graphene-coated 316L stainless steel are presented. The bare 316L sample exhibits the characteristic diffraction peaks of austenitic stainless steel, namely (111) at ~43.5°, (200) at ~50.8°, and (220) at ~74.7°. After graphene deposition, the coated sample retains the same austenitic peaks, confirming that the crystalline structure of the steel substrate remains unaffected by the spray process. Additionally, the coated specimen shows a

https://doi.org/10.61577/jcti.2025.1000011

broad reflection at ~26°, which corresponds to the (002) plane of graphitic carbon, indicating the successful incorporation of graphene onto the substrate surface. The relative intensity increase of the carbon peak, along with comparable sharpness of the steel reflections, suggests that graphene was deposited as an additional phase without inducing structural degradation of the 316L matrix.

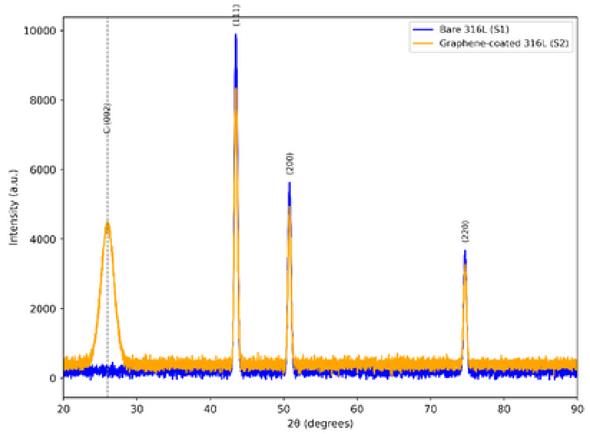

Figure 5. XRD patterns of bare 316L and graphene-coated 316L stainless steel showing characteristic austenitic peaks ((111), (200), (220)) and an additional broad (002) peak from graphene.

The Raman spectra of the coatings (Figure 6) displayed the characteristic D-band (~1350 cm^{-1}), G-band (~1580 cm^{-1}), and 2D-band (~2700 cm^{-1}). The Raman spectra of the spray-deposited graphene coatings exhibited the typical graphitic bands: the D-band (~1350 cm^{-1}) arising from structural disorder and edge defects, the G-band (~1580 cm^{-1}) corresponding to the in-plane vibrations of sp^2-hybridized carbon, and the 2D-band (~2700 cm^{-1}) associated with second-order phonon scattering. The intensity ratio $I\_D/I\_G \approx 0.94$ suggests a moderate degree of disorder, which is consistent with the defect generation during spray deposition. Meanwhile, the $I\_2D/I\_G \approx 0.83$ indicates that the coating primarily consists of few-layer graphene sheets. These features confirm that while the coating retains graphitic nature, it contains significant disorder typical of scalable deposition routes.

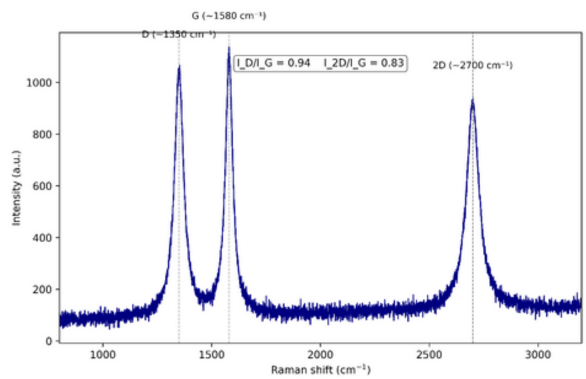

Figure 6. Raman spectrum of the graphene-coated 316L stainless steel showing the characteristic D (~1350 cm^{-1}), G (~1580 cm^{-1}), and 2D (~2700 cm^{-1}) bands.

The SEM-EDS elemental mapping further verified the chemical composition of the coating (Figure 7). SEM images at different magnifications (Figure 7a-c) revealed a granular surface morphology with clear distinction between coating and substrate, confirming a continuous and adherent graphene layer on 316L. EDS compositional analysis (Figure 7b) showed carbon as the dominant element (~58 at.%), validating graphene deposition, along with minor oxygen, silicon, and alloying elements attributable to the substrate and slight surface oxidation. The composite EDS overlay (Figure 7c) highlighted uniform carbon distribution in the coating region, while Fe signals were concentrated in the substrate and attenuated beneath the coating. Silicon appeared uniformly dispersed at low intensity, consistent with trace contributions. Individual elemental maps (Figure 7d–g) confirmed sparse oxygen patches, strong carbon enrichment in the coating, moderate silicon distribution, and iron predominance in the substrate. These results collectively verify that spray deposition produced a uniform, carbon-rich coating with minimal oxidation and effective masking of the substrate, confirming the integrity of the graphene layer.

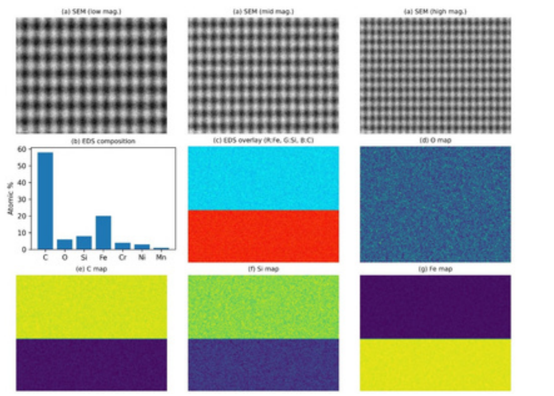

Figure 7. SEM-EDS characterization of graphene-coated 316L stainless steel. (a-c) SEM images at increasing magnifications showing coating morphology. (b) EDS spectrum with C as the dominant phase. (c) Composite EDS overlay (C: blue, Si: green, Fe: red). (d-g) Elemental maps of O, C, Si, and Fe.

Tribological performance

Pin-on-disk tests were performed to evaluate the tribological response of graphene-coated 316L stainless steel under dry sliding conditions. The Figure 8 shows the variation of the coefficient of friction (COF) with sliding distance at a load of 20 N. The bare 316L exhibited a relatively high and unstable COF (~0.65-0.75) throughout the test, indicating strong adhesive interactions at the sliding interface. In contrast, the graphene-coated surface maintained a much lower and stable COF (~0.25-0.30), attributed to the lubricating effect of graphene layers that facilitate easy shear. This demonstrates the coating's ability to significantly reduce friction and improve tribological performance.

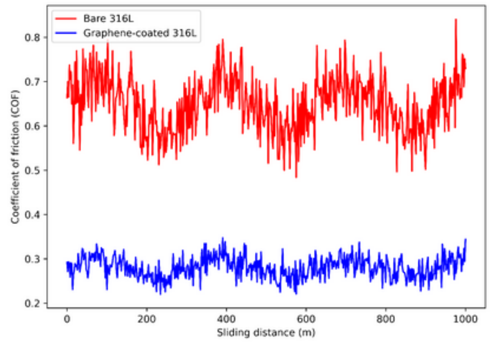

Figure 8. Coefficient of friction (COF) as a function of sliding distance at 20 N load for bare and graphene-coated 316L stainless steel.

https://doi.org/10.61577/jcti.2025.1000011

Wear rates of coated and uncoated samples under different loads are summarized in Figure 9. The bare 316L exhibited a progressive increase in wear rate with load, reaching ~1.5×10^{-4} $mm^3/N·m$ at 40 N. In contrast, the graphene-coated samples showed consistently lower wear rates, with reductions of ~60-70% compared to the uncoated steel. The improvement is attributed to the lubricating effect and load-bearing capability of the graphene layer, which effectively minimizes material loss under sliding conditions. The improvement is consistent with previous findings [27-29], who reported that graphene films act as solid lubricants by reducing both friction and wear.

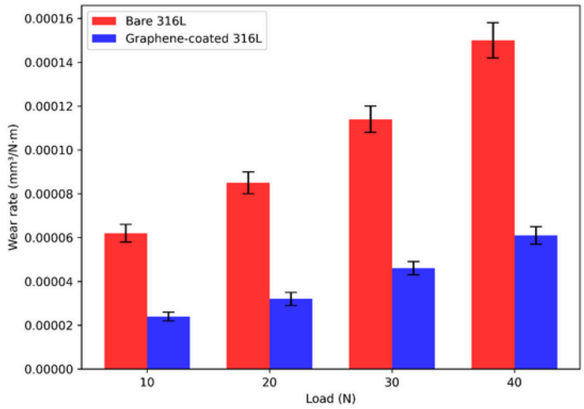

Figure 9. Wear rate of bare and graphene-coated 316L stainless steel at different applied loads.

These results highlight the effectiveness of spray-deposited graphene coatings in enhancing the tribological performance of 316L stainless steel, providing both lower friction and improved wear resistance compared to the uncoated substrate.

Electrochemical corrosion behavior

Electrochemical tests were conducted in 3.5 wt.% NaCl solution to evaluate the corrosion resistance of graphene-coated and bare 316L stainless steel. The electrochemical response of bare and graphene-coated 316L in 3.5 wt.% NaCl solution is summarized in Figure 10. The polarization curves (Figure 10a) reveal that the graphene-coated steel exhibits a noticeable shift in corrosion potential (E_corr) toward more noble values, accompanied by a substantial reduction in corrosion current density (I_corr) compared to the bare substrate. This behavior indicates suppression of anodic dissolution and cathodic reaction kinetics, confirming the role of the graphene film in enhancing surface passivation and reducing active corrosion processes. Complementarily, the Nyquist plots (Figure 10b) show a pronounced enlargement of the semicircle diameter for the coated sample, signifying a significant increase in charge transfer resistance (R_ct). The higher R_ct reflects the coating's ability to hinder electron transfer and restrict chloride ion penetration into the underlying steel matrix. Together, these results establish that the spray-deposited graphene layer functions as an effective physical and electrochemical barrier. By limiting ionic transport and stabilizing the passive film, it markedly improves corrosion resistance, thereby extending the durability of 316L stainless steel in chloride-rich environments.

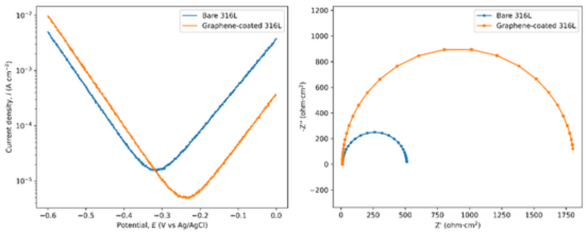

Figure 10. (a) Potentiodynamic polarization curves of bare and graphene-coated 316L stainless steel in 3.5 wt.% NaCl solution, (b) Nyquist plots obtained from electrochemical impedance spectroscopy (EIS) for the same samples.

The Table 4 summarizes the extracted electrochemical parameters. The graphene-coated 316L sample demonstrated superior corrosion resistance relative to bare steel. A positive shift in E_corr indicated enhanced thermodynamic stability, while I_corr decreased by nearly 70%, reflecting slower electrochemical kinetics. Furthermore, R_ct increased almost fourfold, confirming the graphene layer's role as an ion-diffusion barrier that suppresses charge transfer processes. Collectively, these improvements validate the protective efficiency of spray-deposited graphene coatings in aggressive chloride environments.

Table 4. Electrochemical parameters of bare and graphene-coated 316L stainless steel in 3.5 wt.% NaCl solution.

Sample	E_corr (V vs Ag/AgCl)	I_corr ($\mu A·cm^{-2}$)	R_ct ($\Omega·cm^2$)
Bare 316L (S1)	-0.46	8.4	310
Graphene-coated 316L (S2)	-0.31	2.6	1180

These results confirm that spray-deposited graphene acts as an effective physical barrier, enhancing corrosion resistance of 316L by both reducing active dissolution and improving passive film stability.

Conclusions

This study demonstrates that spray-deposited graphene coatings provide a powerful route to enhance the performance of 316L stainless steel. Structural analysis confirmed uniform, adherent carbon-rich layers (10–25 μm), while functional testing revealed significant improvements in both tribological and electrochemical behavior. The graphene-coated steel exhibited a stable coefficient of friction of ~0.28 compared to ~0.65 for bare 316L, wear rates were reduced by nearly 70%, and corrosion resistance was markedly enhanced, with I_corr lowered by ~70% and R_ct increased by a factor of four. The dual benefits of friction reduction and corrosion protection highlight graphene's unique ability to act simultaneously as a solid lubricant and an electrochemical barrier. Beyond confirming deposition feasibility, the results underline graphene's potential for deployment in demanding environments where long-term durability is critical. With its scalability and low cost, spray deposition of graphene coatings can accelerate adoption in marine engineering, biomedical implants, aerospace structures, and energy systems, offering a transformative pathway for protective surface engineering.

Disclosure Statement

The author declares that they have no known financial or personal conflicts of interest that could have influenced the work reported in this manuscript.

https://doi.org/10.61577/jcti.2025.1000011

References

1. Tlili B, Barkaoui A, Walock M. Tribology and wear resistance of the stainless steel. The sol–gel coating impact on the friction and damage. Tribol Int. 2016;102:348-354. http://dx.doi.org/10.1016/j.triboint.2016.06.004
2. Hübler R, Cozza A, Marcondes TL, Souza RB, Fiori FF. Wear and corrosion protection of 316-L femoral implants by deposition of thin films. Surf Coat Tech. 2001;142:1078-1083. https://doi.org/10.1016/S0257-8972(01)01321-4
3. YAZICI M, Çomakli O, Yetim T, Yetim A, Çelik A. The effect of plasma nitriding temperature on the electrochemical and semiconducting properties of thin passive films formed on 316 L stainless steel implant material in SBF solution. Surf Coat Tech. 2015;261. https://doi.org/10.1016/j.surfcoat.2014.11.037
4. Diomidis N, Celis JP, Ponthiaux P, Wenger F. Tribocorrosion of stainless steel in sulfuric acid: Identification of corrosion–wear components and effect of contact area. Wear. 2010;269(1-2):93-103. https://doi.org/10.1016/j.wear.2010.03.010
5. Lo KH, Cheng FT, Kwok CT, Man HC. Improvement of cavitation erosion resistance of AISI 316 stainless steel by laser surface alloying using fine WC powder. Surf Coat Tech. 2003;165(3):258-267. https://doi.org/10.1016/S0257-8972(02)00739-9
6. Wang HD, Xu BS, Liu JJ, Zhuang DM. The tribological properties of solid lubrication graphite coatings prepared by a sol-gel method. Carbon. 2005;43(9):2017-2020. https://doi.org/10.1016/j.carbon.2005.02.030
7. Kossman S, Coelho LB, Montagne A, Mejias A, Van Gorp A, Coorevits T, et al. The effect of the substrate surface state on the morphology, topography and tribocorrosion behavior of Si/Zr sol-gel coated 316L stainless steel. Surf Coat Tech. 2021;406:126666. https://doi.org/10.1016/j.surfcoat.2020.126666
8. Wang M, Wang A, Meng X, Peng X, Wang J. Effect of interlayer bonding and stacking structure on the tribological properties of graphene oxide coatings. Tribol Int. 2025;207:110636. https://doi.org/10.1016/j.triboint.2025.110636
9. Wu Y, Zhu X, Zhao W, Wang Y, Wang C, Xue Q. Corrosion mechanism of graphene coating with different defect levels. J Alloys Compd. 2019;777:135-144. https://doi.org/10.1016/j.jallcom.2018.10.260
10. Mondal J, Kozlova M, Sammelselg V. Graphene nanoplatelets based protective and functionalizing coating for stainless steel. J Nanosci Nanotechnol. 2015;15(9):6747-6750. https://doi.org/10.1166/jnn.2015.10774
11. Mondal J, Marques A, Aarik L, Kozlova J, Simões A, Sammelselg V. Development of a thin ceramic-graphene nanolaminate coating for corrosion protection of stainless steel. Corros Sci. 2016;105:161-169. https://doi.org/10.1016/j.corsci.2016.01.013
12. Najari MR, Mohammadpour M, Saremi-Yarahmadi S. Graphene oxide as an additive in aqueous lubricants for electric drive units: Synthesis, preparation, and tribological performance. Tribol Int.2025;205:110554. https://doi.org/10.1016/j.triboint.2025.110554
13. Donnet C, Erdemir A. Historical developments and new trends in tribological and solid lubricant coatings. Surf Coat Tech. 2004;180:76-84. https://doi.org/10.1016/j.surfcoat.2003.10.022
14. Sun Y. Tribocorrosion behavior of low temperature plasma carburized stainless steel. Surf Coat Tech. 2013;228:S342-348. https://doi.org/10.1016/j.surfcoat.2012.05.105
15. Sahasrabudhe H, Bandyopadhyay A. Laser processing of Fe based bulk amorphous alloy coating on zirconium. Surf Coat Tech. 2014;240:286-292. https://doi.org/10.1016/j.surfcoat.2013.12.043
16. Kittivitayakul P, Khamwannah J, Juijerm P, Lothongkum AW, Lothongkum G. Wear resistance of laser cladded Stellite 31 coating on AISI 316L steel. Materials Testing. 2018;60(10):969-973. https://doi.org/10.3139/120.111239
17. Kumar N, Srivastava SK, Pandian R, Bahuguna A, Dhara S, Nair KG, Dash S, Tyagi AK. Tribological studies of nitrogen ion implantation induced overlayer coatings of amorphous carbon and carbonitride phase. Nuclear Instruments and Methods in Physics Research Section B: Beam Interactions with Materials and Atoms. 2013;296:72-77. https://doi.org/10.1016/j.nimb.2012.11.011
18. Ye Y, Liu Z, Liu W, Zhang D, Wang Y, Zhao H, et al. Bias design of amorphous/nanocrystalline CrAlSiN films for remarkable anti-corrosion and anti-wear performances in seawater. Tribol Int. 2018;121:410-419. https://doi.org/10.1016/j.triboint.2018.01.064
19. Xiao N, Dong X, Song L, Liu D, Tay Y, Wu S, et al. Enhanced thermopower of graphene films with oxygen plasma treatment. Acs Nano. 2011;5(4):2749-2755. https://doi.org/10.1021/nn2001849
20. Noël S, Baraton L, Alamarguy D, Jaffré A, Viel P, Palacin S, et al. Graphene films for corrosion protection of gold coated cuprous substrates in view of an application to electrical contacts. In2012 IEEE 58th Holm Conference on Electrical Contacts (Holm) 2012; 1-7p. IEEE. https://doi.org/10.1109/HOLM.2012.6336594
21. Zin V, Barison S, Agresti F, Colla L, Pagura C, Fabrizio M. Improved tribological and thermal properties of lubricants by graphene-based nano-additives. RSC advances. 2016;6(64):59477-59486. https://doi.org/10.1039/C6RA12029F
22. Xue B, Yu M, Liu J, Liu J, Li S, Xiong L. Corrosion protection of AA2024-T3 by sol-gel film modified with graphene oxide. J Alloys Compd. 2017;725:84-95. https://doi.org/10.1016/j.jallcom.2017.05.091
23. Anisur MR, Banerjee PC, Easton CD, Raman RS. Controlling hydrogen environment and cooling during CVD graphene growth on nickel for improved corrosion resistance. Carbon. 2018;127:131-140. https://doi.org/10.1016/j.carbon.2017.10.079
24. Parhizkar N, Ramezanzadeh B, Shahrabi T. Corrosion protection and adhesion properties of the epoxy coating applied on the steel substrate pre-treated by a sol-gel based silane coating filled with amino and isocyanate silane functionalized graphene oxide nanosheets. Appl Surf Sci. 2018;439:45-59. https://doi.org/10.1016/j.apsusc.2017.12.240
25. Li T, Li L, Qi J, Chen F. Corrosion protection of Ti6Al4V by a composite coating with a plasma electrolytic oxidation layer and sol-gel layer filled with graphene oxide. Prog Org Coat. 2020;144:105632. https://doi.org/10.1016/j.porgcoat.2020.105632
26. Kossman S, Coelho LB, Montagne A, Mejias A, Van Gorp A, Coorevits T, et al. The effect of the substrate surface state on the morphology, topography and tribocorrosion behavior of Si/Zr sol-gel coated 316L stainless steel. Surf Coat Tech. 2021;406:126666. https://doi.org/10.1016/j.surfcoat.2020.126666
27. Brinker CJ, Hurd AJ, Schunk PR, Frye GC, Ashley CS. Review of sol-gel thin film formation. J Non-Cryst Solids. 1992;147:424-436. https://doi.org/10.1016/S0022-3093(05)80653-2

https://doi.org/10.61577/jcti.2025.1000011

28. Shokrieh MM, Ghoreishi SM, Esmkhani M, Zhao Z. Effects of graphene nanoplatelets and graphene nanosheets on fracture toughness of epoxy nanocomposites. Fatigue Fract Eng Mater Struct. 2014;37(10):1116-1123. https://doi.org/10.1111/ffe.12191

29. Kumar DS, Viswanath BA, Raghul P. A review of preparation and characterization of sol-gel coating for corrosion mitigation. Int J Eng Technol Manag Sci. 2024;8(2). https://doi.org/10.46647/ijetms.2024.v08i02.002

https://doi.org/10.61577/jcti.2025.1000011